Brief communication: Use of lightweight and low-cost steel net electrodes for electrical resistivity tomography (ERT) surveys performed on coarse-blocky surface environments

Mirko Pavoni [1], L. Peruzzo [1], J. Boaga [1], A. Carrera [1], I. Barone [1] and A. Bast [2,3]

[1] Department of Geosciences, Università degli Studi di Padova, Padova, Italy.
[2] WSL Institute for Snow and Avalanche Research SLF, Permafrost Research Group, Davos Dorf, Switzerland.
[3] Climate Change, Extremes and Natural Hazards in Alpine Regions Research Center CERC, Davos Dorf, Switzerland.

Correspondence to: Mirko Pavoni (mirko.pavoni@unipd.it)

Abstract. ERT is a widely used geophysical technique for characterizing various mountainous environments where land surfaces consist of coarse blocks and debris (e.g., rock glaciers). In these conditions, installing steel spike electrodes is both challenging and time-consuming, and achieving acceptable grounding resistance between the electrodes and the surface is difficult. In this work, we successfully tested the performance and the durability of an alternative electrode that is more robust, lightweight, and cost-effective than the recently proposed textile electrode. A stainless-steel net and sponge are used to create small bags that can be easily inserted between the blocks and later removed.

1 Introduction

Electrical Resistivity Tomography (ERT) is one of the most widely used geophysical methods for the characterization of various study environments (e.g., Boaga et al., 2018; Deiana et al., 2022; Carrera et al., 2024; Pavoni et al., 2024; Peruzzo et al., 2024), as data acquisition is generally rapid and relatively straightforward (Binley, 2015). Thanks to the development of reliable open-source inversion techniques, the distribution of electrical properties in the subsurface can be efficiently reconstructed (Rücker et al., 2017). The reliability of resistivity models is closely linked to the quality of acquired data, which in turn depends on achieving good electrical contact between electrodes and soil (Pavoni et al., 2022). This resistance is part of the overall grounding resistance, which depends on soil resistivity, electrode geometry, and the quality of contact with the ground. Grounding resistance plays a crucial role in ensuring effective current injection and reliable ERT measurements (Binley and Slater, 2020). For this reason, modern electrical resistivity meters perform an automated check before acquisition by injecting a low current through each electrode, measuring the resulting voltage drop to estimate electrode resistance, and identifying poorly coupled electrodes. Therefore, electrodes must be made from highly conductive materials. Common choices include graphite, copper, and stainless steel (Rücker and Günther, 2011). Graphite offers low resistance but poor mechanical performance. Copper has excellent conductivity but tends to oxidize, reducing effectiveness over time. Stainless steel, though less conductive, does not oxidize, has good mechanical strength, and is cost-effective (Reynolds, 2011). For these reasons, stainless-steel spike electrodes, typically 30–40 cm in length and 1–2 cm in diameter, are widely used in ERT surveys (Rücker and Günther, 2011). While easy to install in fine soils, their deployment in coarse-blocky terrains such as landslide deposits or rock glaciers is often difficult and time-consuming (Bast et al., 2024). Removal can also be problematic when electrodes become embedded between blocks. Even when physical contact is good, sponges soaked in salt water are often used to reduce contact resistance (Pavoni et al., 2022).

To facilitate the installation of ERT arrays in rock glaciers, Buckel et al. (2023) proposed an alternative electrode consisting of a conductive textile sachet filled with sand (Mudler et al., 2021). These fist-sized electrodes can be easily inserted between blocks, wetted with salt water, and removed after use. Their performance was tested by Bast et al. (2024), confirming their reliability. However, the conductive textile used in both studies contains copper and nickel, which are prone to oxidation,

39   potentially reducing performance over time (Bast et al., 2024). Moreover, each electrode costs approximately €15 and weighs

40   around 250–300 g, making it relatively expensive and heavy.

41   In this work, we propose a lightweight stainless-steel net electrode filled with a carwash sponge. This design uses oxidation-

42   resistant material, significantly reduces weight and cost, and improves the mechanical robustness of the electrode compared

43   to textile-based solutions. We tested the performance of the newly developed stainless-steel net electrode by conducting ERT

44   surveys at the same coarse-blocky sites used by Bast et al. (2024), and compared the results with those obtained using

45   traditional stainless-steel spikes coupled with sponges. In addition, we tested their long-term performance by employing them

46   on a permanent ERT monitoring line installed on a rock glacier.

2 Site description

48   The proposed stainless-steel net electrodes were tested in typical high mountain environments characterized by coarse blocky

49   and debris-covered surfaces, including a landslide deposit (Marocche di Drò), an inactive rock glacier (Sadole rock glacier),

50   and an active rock glacier (Flüela rock glacier). For detailed site descriptions, maps, and images, we refer to Bast et al. (2024).

51   The landslide deposit known as the Marocche di Drò (Trentino, Italy; 45.983° N, 10.941° E) consists of a chaotic surface

52   accumulation of calcareous blocks and debris (limestone), underlain by a more heterogeneous sedimentary body (Weidinger

53   et al., 2014). The test survey was carried out along the same profile previously investigated by Bast et al. (2024).

54   The Sadole rock glacier (Trentino, Italy; 46.242° N, 11.592° E) features a surface dominated by large blocks and coarse debris

55   of ignimbritic volcanic origin (Pavoni et al., 2023). According to Bast et al. (2024), the central lobe hosts a frozen layer at

56   approximately 10 m depth. Our comparison test was conducted along the first half of their original survey line.

57   The Flüela rock glacier (Grisons, Switzerland; 46.746° N, 9.951° E) is characterized by a chaotic mixture of metamorphic

58   blocks and boulders (amphibolites and paragneisses), with some interspersed patches of finer sediments (Boaga et al., 2024).

59   The comparative measurements were performed along the upper section of the profile investigated by Bast et al. (2024).

3 Methods

3.1 Stainless steel-net electrodes

62   To replicate the size of the textile electrode (Mudler et al., 2021, Buckel et al., 2023), each stainless-steel net electrode was

63   constructed by cutting 35×35 cm square sheets from a thin commercial stainless-steel mesh (Fig. 1a). The net was shaped into

64   a fist-sized pouch filled with a car-wash sponge and sealed using a standard electrician's cable tie. Each electrode weighs

65   approximately 50 g, i.e., one-fifth the weight of traditional stainless-steel spike or textile electrodes, and the material cost is

66   around € 3–4, i.e., one-quarter of the cost of textile electrode design.

3.2 Data acquisition

68   ERT data were collected using a Syscal Pro resistivity meter (Iris Instruments, Orléans, France; www.iris-instruments.com)

69   with 24-electrode arrays and site-specific electrode spacings: 5 m at Marocche di Drò, 3.5 m at Sadole, and 2 m at Flüela. A

70   dipole–dipole acquisition scheme was adopted with variable electrode skips, as described in Pavoni et al. (2023), and included

71   reciprocal measurements, i.e., with current and potential dipoles interchanged (Binley and Slater, 2020).

72   For each survey line, measurements were performed using traditional stainless-steel spike electrodes (combined with sponges;

73   Fig. 1b), and then repeated using the proposed stainless-steel net electrodes (Fig. 1c). In both cases, saltwater was applied to

74   improve the galvanic contact between the electrodes and the coarse blocky surface (Pavoni et al., 2022). The two electrode

75   types were installed in the same locations between blocks and boulders (Fig. 1b–c), with approximately 0.5 L of saltwater

76   poured on each electrode prior to acquisition.

77 At the Sadole rock glacier site, net electrodes were installed for a permanent ERT monitoring line to assess their long-term

78 performance. We compared measurements (grounding resistance, injected current, and reciprocal error) acquired in June 2024

79 and June 2025.

80 **3.3 Data processing**

81 At each test site, grounding resistance was measured prior to data acquisition for both electrode types. To compare these values,

82 grounding resistance measurements from each electrode pair were visualized using histograms. Dataset quality was assessed

83 by calculating the reciprocal error for each quadrupole (Tso et al., 2017), and histograms were also used to compare the

84 distribution of injected currents and reciprocal errors across the different electrode types.

85 The apparent resistivity pseudosections were compared by calculating the differences in measured resistance values between

86 the two datasets. Additionally, apparent resistivity values were analysed using scatterplots with linear regression lines and

87 corresponding R^2 values. Each dataset was filtered using a reciprocal error threshold to ensure a homogeneous distribution of

88 data points across the profile (Pavoni et al., 2023). This value was used as expected data error in the inversion process, which

89 was carried out using the open-source software ResIPy (Blanchy et al., 2020). Note that, only the quadrupoles common to both

90 datasets after filtering were used for the inversion process (Bast et al., 2024). The resulting inverted resistivity models were

91 then compared by analysing both the section images and the cell-wise resistivity values from the inversion mesh using

92 scatterplots with regression lines and R^2 values.

93 **4 Results and interpretation**

94 In the comparative test at the Marocche di Drò site, the grounding resistances measured with the two types of electrodes were

95 very similar (Fig. 2a), with values < 200 kΩ (most being < 100 kΩ), ensuring acceptable conditions to acquire ERT

96 measurements in this challenging environment (Pavoni et al., 2022). These favorable resistance values also resulted in optimal

97 injected currents, which were consistently above 3 mA, as shown in Fig. 2b. This is further confirmed by the quality of the

98 acquired data: most of the measured quadrupoles (85% for spike and 90% for net electrodes) show a reciprocal error < 5%

99 (Fig. 2c), which was chosen as a threshold to filter the datasets and used as the expected error in the inversion processes. As

100 highlighted in the scatterplots (Fig. 3a and 3g), there is a very high correlation between the measured apparent resistivities and

101 the inverted resistivities, both showing $R^2 = 0.99$. The obtained apparent (Fig. 3d) and inverted resistivity sections (Figs. 3j

102 and 3m) are nearly identical and allow for the reconstruction of the known structure of the landslide deposit (Weidinger et al.,

103 2014), where large blocks with extensive air voids are characterized by high resistivity values near the surface. At greater

104 depths, resistivity values decrease significantly, confirming the presence of more heterogeneous and finer sediments.

105 At the Sadole rock glacier, the measured grounding resistances were significantly improved using the net-electrodes (Fig. 2d).

106 With the spike-electrodes array, almost half of the grounding resistances have values > 100 kΩ, and > 50 % of the values are

107 higher > 200 kΩ. In contrast, in the case of net electrodes, the grounding resistance values are clearly lower, which enables the

108 injection of higher currents (fig. 2e) and consequently the acquisition of a higher-quality dataset (Fig. 2e). In the dataset

109 acquired with the net electrodes, more than half of the quadrupoles exhibit a reciprocal error below 1%, and only four

110 quadrupoles exceed 5%. Nonetheless, the spike electrodes also yielded a high-quality dataset, with 90% of the quadrupoles

111 showing a reciprocal error below 5%. Despite these minor differences in data quality, the same filtering threshold (reciprocal

112 error > 5%) was applied to both datasets and used as the expected data error during the inversion process. As illustrated in

113 Figures 3b and 3e, the measured apparent resistivities and the corresponding inverted values exhibit a strong correlation, albeit

114 slightly lower than at the Marocche di Drò site ($R^2 = 0.91$ for apparent resistivities and $R^2 = 0.93$ for inverted values). Once

115 again, the apparent (Fig. 3e) and inverted resistivity sections (Figs. 3k and 3n) are nearly identical and clearly reveal the

116 presence of a high-resistivity frozen layer at approximately 10 m depth (Bast et al., 2024).

117 The measured grounding resistances at the Flüela rock glacier site (Fig. 2g) were generally higher than at the other two sites.
118 With both electrode types, more than half of the electrodes exhibited grounding resistances > 200 kΩ. As a consequence, the
119 injected currents (Fig. 2h) were consistently lower compared to those recorded at the Marocche di Drò and Sadole sites. This
120 is reflected in the dataset quality (Fig. 2i), where only 78% of the acquired quadrupoles in both datasets exhibit a reciprocal
121 error < 5%, and 90% remain below 10%, which was adopted as the expected error for the inversion process. The correlation
122 between apparent resistivities obtained using the two electrode types is also lower than at the other sites (Fig. 3c, R^2 = 0.80).
123 Accordingly, the inverted resistivities from the resulting models show a reduced correlation as well (R^2 = 0.88; Fig. 3i). Despite
124 minor differences, both the apparent (Fig. 3f) and inverted resistivity sections (Figs. 3l and 3o) derived from the two electrode
125 types consistently delineate the same subsurface structure: a high-resistivity permafrost body a few meters below the surface
126 in the first half of the profile (x < 20 m). Variations appear at greater depths, where resistivities in Fig. 3l are higher than in
127 Fig. 3o, and toward the front of the array (x > 25 m), where lower values indicate unfrozen ground.
128 Finally, Figures 2j–2l clearly show that, despite the net electrodes being left in situ (Sadole rock glacier) for over a year, their
129 performance remained essentially unchanged. They allowed for the acquisition of comparable grounding resistance values and
130 injected currents, as well as similar reciprocal errors in the datasets collected in June 2024 and June 2025.

131 **4 Discussion and conclusions**

132 The results confirm that lower grounding resistance enhances current injection and improves ERT data quality (Pavoni et al.,
133 2022). The Marocche di Drò site exhibited optimal conditions, characterized by minimal grounding resistance, highest injected
134 currents, and improved data quality. Similarly, the Sadole site showed relatively low grounding resistance and consistently
135 high-quality data. In contrast, the Flüela site presented moderately higher grounding resistance, resulting in reduced injected
136 current and lower data quality; nevertheless, datasets remained suitable for processing after applying a 10% reciprocal error
137 threshold, an acceptable criterion given the site's challenging surface conditions.
138 These variations likely reflect differences in subsurface lithologies: limestone at the Marocche site facilitates galvanic contact
139 more effectively than ignimbrite (Sadole site) or paragneiss (Flüela site) (Duba et al., 1978). Moreover, sites with lower
140 grounding resistance and higher data quality exhibited stronger correlations between apparent and inverted resistivities across
141 electrode types. At Marocche di Drò, results obtained with both electrode types showed excellent agreement. At Sadole, the
142 correlation between datasets remained high despite a slight decrease in data quality. At Flüela, correlation further declined;
143 however, inverted resistivity models consistently resolved the near-surface permafrost structure.
144 Overall, the proposed stainless steel-net electrodes perform comparably to traditional steel spikes, providing a lightweight,
145 low-cost, and reliable solution for ERT surveys in coarse-blocky terrains. They retain the operational advantages of textile
146 electrodes, such as ease of insertion and removal between blocks, while overcoming critical limitations identified by Bast et
147 al. (2024), including greater durability due to oxidation resistance, reduced cost and weight, and enhanced mechanical
148 robustness. Finally, long-term monitoring at the Sadole site further confirmed stable electrode performance over one year,
149 supporting their suitability for permanent ERT installations targeting permafrost monitoring. In contrast, textile electrodes are
150 unsuitable for long-term applications due to oxidation issues and limited durability.
151 A potential strategy to facilitate electrode transport involves carrying only the steel net or conductive textile sheets to the rock
152 glacier and assembling the electrode bags in situ using locally sourced fine material. This approach could reduce transport
153 volume—and weight in the case of textile electrodes—but requires a substantial time investment to procure adequate fine
154 material on-site, which is rarely abundant in rock glacier environments, as well as to assemble 48 to 96 electrodes in the field,
155 potentially impacting fieldwork efficiency.
156 Future work will investigate the applicability of stainless steel-net electrodes for induced polarization measurements in both
157 time and frequency domains.
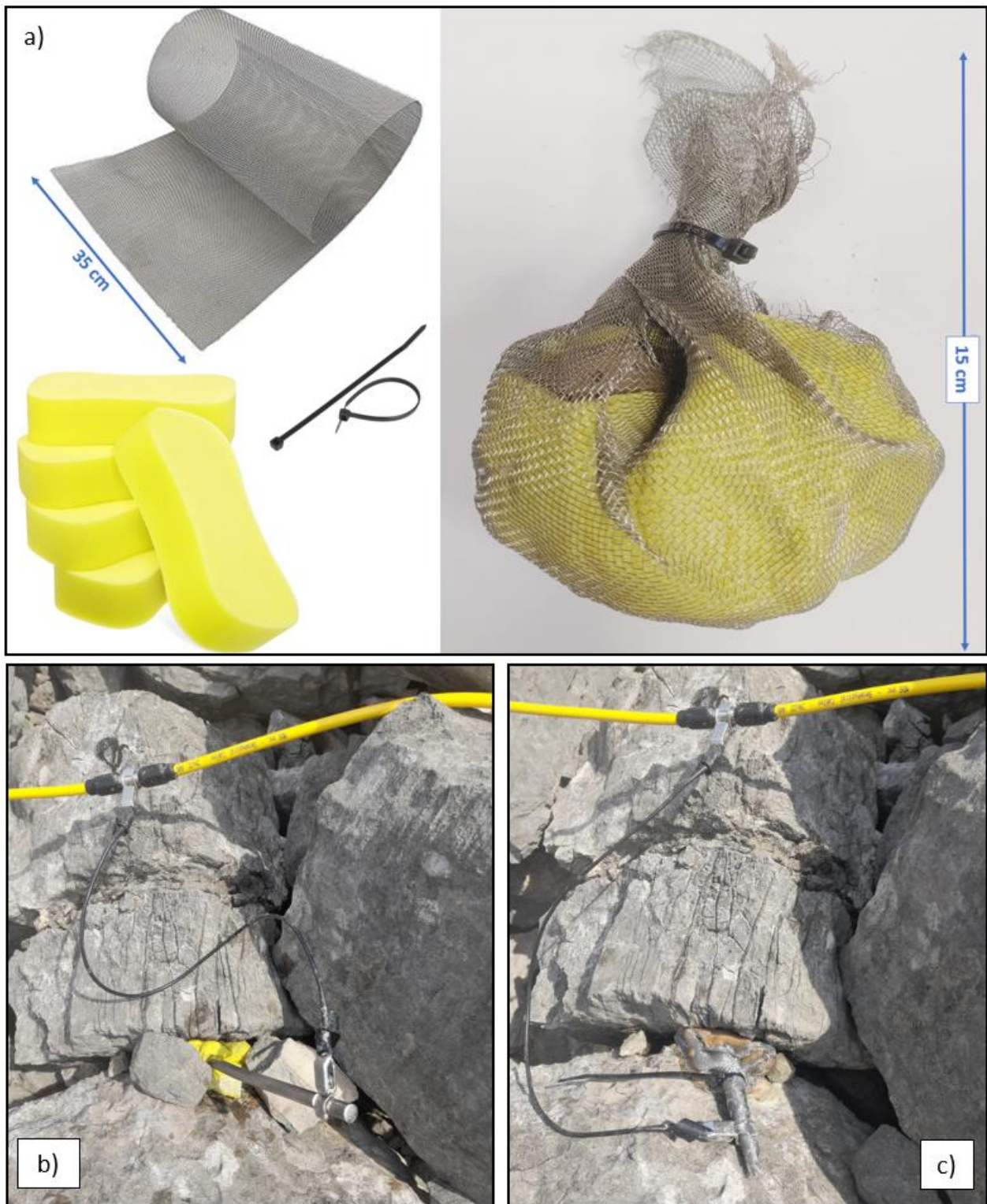
158

159 **Figure 1: (a) Stainless steel net electrode assembled by cutting 35 × 35 cm squares from a thin commercial mesh, inserting a car-**
160 **wash sponge, and securing the unit with a cable tie. (b) Traditional stainless steel spike electrode with a saltwater-soaked sponge, as**
161 **used at the Marocche di Drò site. (c) Proposed stainless steel net electrode, also moistened with salt water, deployed at the same site.**
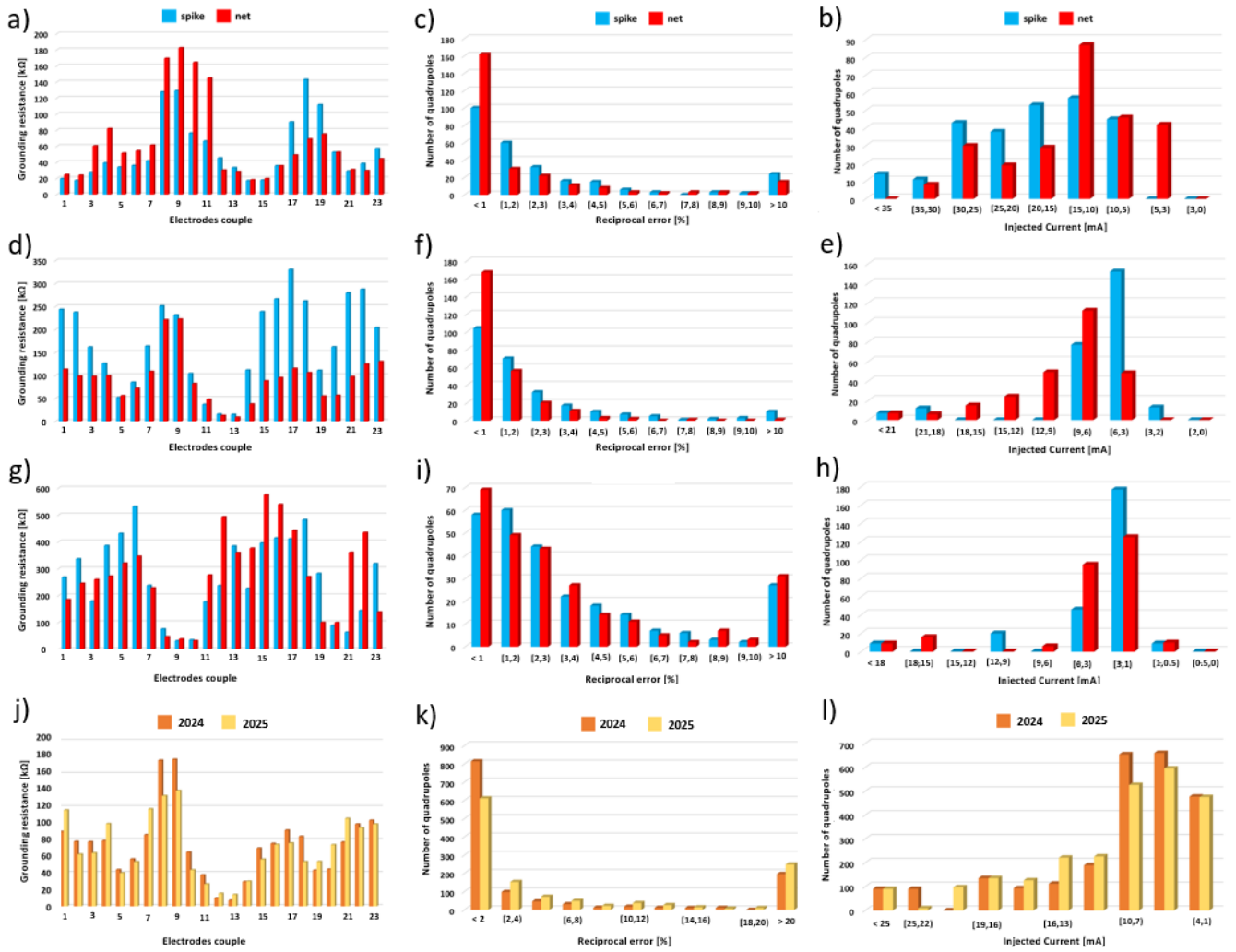
162
163 **Figure 2. Histograms (a), (d), and (g) compare grounding resistances [kΩ] recorded at the Marocche di Drò, Sadole, and Flüela test**
164 **sites, respectively, using traditional stainless-steel spike electrodes with sponges (blue) and the proposed stainless-steel net electrodes**
165 **with sponge inserts (red). Panels (b), (e), and (h) show the corresponding injected electric currents [mA], while (c), (f), and (i) present**
166 **the reciprocal error [%] of the quadrupoles for the same sites and electrode types. All electrodes were moistened with the same**
167 **amount of saltwater and placed at comparable positions between surface boulders (see Fig. 1b–c). Panels (j), (k), and (l) illustrate**
168 **the contact resistances (first 24 electrodes, as in panel a), injected currents, and reciprocal errors for datasets acquired at the Sadole**
169 **site in June 2024 (orange) and June 2025 (yellow) along the permanent ERT monitoring line using the stainless-steel net electrodes.**
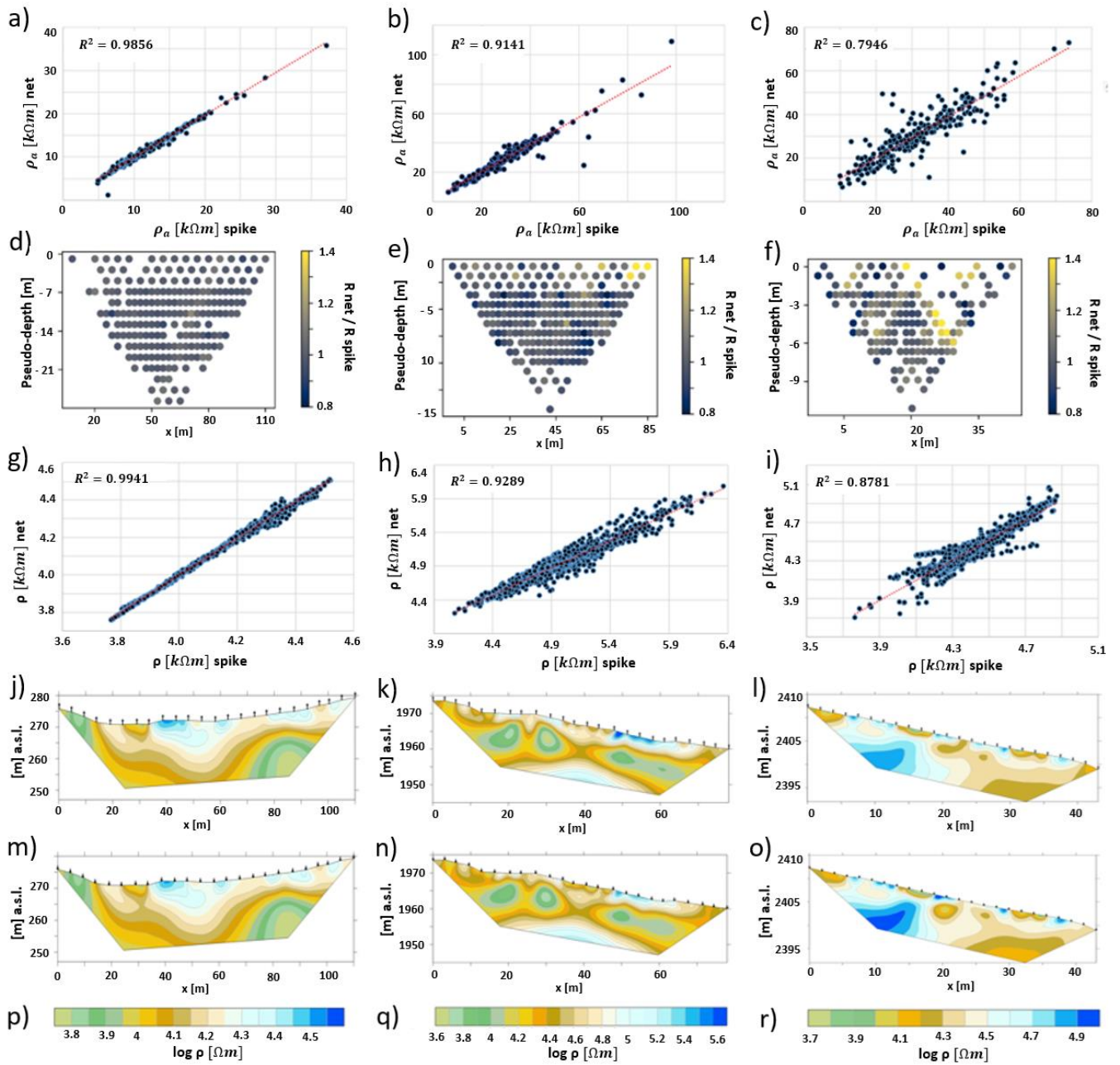
Figure 3. a) Scatterplot comparing apparent resistivity values (ρ_a) measured at the Marocche di Drò site using traditional stainless-steel spike electrodes (with sponges) and the proposed stainless-steel net electrodes. Red dashed lines indicate linear regressions, with corresponding R^2 values. d) Pseudosection showing the ratio of resistance values measured with spike electrodes to those measured with net electrodes, based on the common quadrupoles retained after data filtering for inversion. g) Scatterplot comparing inverted resistivity values (ρ) obtained from the two datasets at Marocche di Drò. Red dashed lines represent regression lines; R^2 values are shown. j) Inverted resistivity model derived from the spike-electrode dataset at Marocche di Drò. m) Inverted resistivity model derived from the net-electrode dataset at Marocche di Drò. p) Color scale used for the inverted resistivity models at the Marocche di Drò site. b), e), h), k), n), and q) correspond to a), d), g), j), m), and p), respectively, for the Sadole rock glacier test site. c), f), i), l), o), and r) correspond to a), d), g), j), m), and p), respectively, for the Flüela rock glacier test site.

187 *Data Availability Statement.* The datasets used to obtain the results presented in this work are available in the open-source
188 repository https://zenodo.org/records/14651003. Furthermore, the ERT datasets will also be included in the International
189 Database of Geoelectrical Surveys on Permafrost (IDGSP).

190 *Author contributing.* MP initiated and conceptualised the study concept and performed the data processing. All authors were

191 involved in the data acquisition and contributed to the writing and editing of the manuscript.

192 *Competing interests:* The contact author has declared that none of the authors has any competing interests.

193 *Financial support:* This study was carried out within the project of the excellence program: "The Geosciences for Sustainable

194 Development" project (Budget Ministero dell'Università e della Ricerca–Dipartimenti di Eccellenza 2023–2027

195 C93C23002690001), and within the project PRIN 2022 "SUBSURFACE – Ecohydrological and environmental significance

196 of subsurface ice in alpine catchments" (code no. 2022AL7WKC, CUP: C53D23002020006), which received funding from

197 the European Union NRRP (Mission 4, Component 2, Investment 1.1 – D. D. 104 2/2/2022).

198

199 *Acknowledgements:* We thank the editor, Professor Hördt, and two anonymous reviewers for their constructive comments and

200 useful suggestions.

References

202 Bast, A., Pavoni, M., Lichtenegger, M., Buckel, J., and Boaga, J.: The Use of Textile Electrodes for Electrical Resistivity
203 Tomography in Periglacial, Coarse Blocky Terrain: A Comparison With Conventional Steel Electrodes. Permafrost and
204 Periglacial Processes, https://doi.org/10.1002/ppp.2257, 2024.

205 Binley, A.: Tools and Techniques: Electrical Methods, Treatise on Geophysics: Second Edition. Elsevier B.V.
206 https://doi.org/10.1016/B978-0-444-53802-4.00192-5, 2015.

207 Binley, A., and Slater, L.: Resistivity and induced polarization: Theory and applications to the near-surface earth. Cambridge
208 University Press, DOI: 10.1017/9781108685955, 2020.

209 Blanchy, G., Saneiyan, S., Boyd, J., McLachlan, P., and Binley, A.: ResIPy, an intuitive open source software for complex
210 geoelectrical inversion/modeling. Computers & Geosciences, 137, 104423, https://doi.org/10.1016/j.cageo.2020.104423,
211 2020.

212 Boaga, J., Pavoni, M., Bast, A., and Weber, S.: Brief communication: On the potential of seismic polarity reversal to identify
213 a thin low-velocity layer above a high-velocity layer in ice-rich rock glaciers. The Cryosphere, 18(7), 3231-3236,
214 https://doi.org/10.5194/tc-18-3231-2024, 2024.

215 Boaga, J., Ghinassi, M., D'Alpaos, A., Deidda, G. P., Rodriguez, G., and Cassiani, G.: Geophysical investigations unravel the
216 vestiges of ancient meandering channels and their dynamics in tidal landscapes. Scientific Reports, 8(1), 1708,
217 DOI:10.1038/s41598-018-20061-5, 2018.

218 Buckel, J., Mudler, J., Gardeweg, R., Hauck, C., Hilbich, C., Frauenfelder, R., Kneisel, C., Buchelt, S., Blöthe, J. H., Hördt,
219 A., and Bücker, M.: Identifying mountain permafrost degradation by repeating historical electrical resistivity tomography
220 (ERT) measurements, The Cryosphere, 17, 2919–2940, https://doi.org/10.5194/tc-17-2919-2023, 2023.

221 Carrera, A., Peruzzo, L., Longo, M., Cassiani, G., and Morari, F.: Uncovering soil compaction: performance of electrical and
222 electromagnetic geophysical methods. SOIL, 10(2), 843–857, https://doi.org/10.5194/soil-10-843-2024, 2024.

223 Deiana, R., Deidda, G. P., Cusí, E. D., van Dommelen, P., and Stiglitz, A.: FDEM and ERT measurements for archaeological
224 prospections at Nuraghe S'Urachi (West-Central Sardinia). Archaeological Prospection, 29(1), 69-86.
225 https://doi.org/10.1002/arp.1838, 2022.

226 Duba, A., Piwinskii, A. J., Santor, M., and Weed, H. C.: The electrical conductivity of sandstone, limestone and granite.
227 Geophysical Journal International, 53(3), 583-597, https://doi.org/10.1111/j.1365-246X.1978.tb03761.x, 1978.

228 Mudler, J., Buckel, J., Bücker, M., and Hördt, A., 2021. Elektrode mit leitfähigem Textilmaterial zur elektrischen
229 Widerstandsmessung des Untergrundes. Patent DE 10 2021 110 721.

230 Pavoni, M., Carrera, A., and Boaga, J.: Improving the galvanic contact resistance for geoelectrical measurements in debris
231 areas: A case study. Near Surface Geophysics, 20(2), 178-191, https://doi.org/10.1002/nsg.12192, 2022.

232 Pavoni, M., Boaga, J., Carrera, A., Zuecco, G., Carturan, L., and Zumiani, M.: Brief communication: Mountain permafrost
233 acts as an aquitard during an infiltration experiment monitored with electrical resistivity tomography time-lapse measurements.
234 The Cryosphere, 17(4), 1601-1607, https://doi.org/10.5194/tc-17-1601-2023, 2023.

235 Pavoni, M., Boaga, J., Peruzzo, L., Barone, I., Mary, B., & Cassiani, G.: Characterization of a Contaminated Site Using Hydro-
236 Geophysical Methods: From Large-Scale ERT Surface Investigations to Detailed ERT and GPR Cross-Hole Monitoring.
237 Water, 16(9), 1280, https://doi.org/10.3390/w16091280, 2024.

238 Peruzzo, L., Chou, C., Hubbard, S., Brodie, E. L., Uhlemann, S., Dafflon, B., and Wu, Y.: Outdoor Mesoscale Fabricated
239 Ecosystems: Rationale, Design, and Application to Evapotranspiration. Design, and Application to Evapotranspiration,
240 https://doi.org/10.1016/j.scitotenv.2024.177565, 2024.

241 Reynolds, J. M.: An introduction to applied and environmental geophysics. John Wiley & Sons, ISBN 9778-0-471-48535-3,
242 2011.

243 Rücker, C., and Günther, T.: The simulation of finite ERT electrodes using the complete electrode model. Geophysics, 76(4),
244 F227-F238. https://doi.org/10.1190/1.3581356, 2011.

245 Rücker, C., Günther, T., and Wagner, F. M.: pyGIMLi: An open-source library for modelling and inversion in geophysics.
246 Computers & Geosciences, 109, 106-123, https://doi.org/10.1016/j.cageo.2017.07.011, 2017.

247 Tso, C. H. M., Kuras, O., Wilkinson, P. B., Uhlemann, S., Chambers, J. E., Meldrum, P. I., ... and Binley, A..: Improved
248 characterisation and modelling of measurement errors in electrical resistivity tomography (ERT) surveys. Journal of Applied
249 Geophysics, 146, 103-119, https://doi.org/10.1016/j.jappgeo.2017.09.009, 2017.

250 Weidinger, J.T., Korup, O., Munack, H., Altenberger, U., Dunning, S.A., Tippelt, G., and Lottermoser, W.: Giant rock slides
251 from the inside. Earth and Planetary Science Letters 389, 62–73, https://doi.org/10.1016/j.epsl.2013.12.017, 2014.